MME 2009

20th Micromechanics Europe Workshop

20-22 September 2009, Toulouse, France

1989 Miko ELWENSPOEK NED	1990 Ernst OBERMEIER GER	2002 Alexandru MULLER ROU	2003 Reinoud WOLFFENBUTTEL NED	2004 Robert PUERS BEL
	1992 Robert PUERS BEL	2001 Martin HILL IRL		2005 Peter ENOKSSON SWE
1994 Paolo DARIO ITA	1993 Nico DE ROOIJ SUI	2000 Ylva BÄCKLUND SWE		2006 Hywel MORGAN ENG
1995 Otto LEISTICO DEN		1999 Alain BOSSEBOEUF FRA		2007 Jose HIGINO CORREIA POR
1996 Juan MORANTE ESP	1997 Alan EVANS ENG	1998 Per OHLCKERS NOR	2009 Patrick PONS FRA	2008 Uwe SCHNAKENBERG GER

LAAS-CNRS

A18 (ID 131)
Ferrous MEMS gradiometers: A comparative study
Humberto Campanella1, R.P. del Real2, Marina Díaz-Michelena2, Marta Duch1, Héctor Guerrero2, Jaume Esteve1, José A. Plaza1
1 Instituto de Microelectrònica de Barcelona (Spain)
2 Instituto Nacional de Técnica Aeroespacial Manuel Terradas (Spain)

A19 (ID 135)
Hollow Microneedles for Pain-Free Drug Delivery
J. O'Brien1, M. Bedoni2-3, A. Blake1, J. Scully1, E. Forvi2-4, M. Casella2-5, F. Gramatica2, and C.O'Mahony1
1 Tyndall National Institute (Ireland)
2 Don Gnocchi Foundation (Italy)
3 Milan University (Italy)
4 Politecnico of Milan (Italy)
5 Magna Graecia University (Italy)

A20 (ID 136)
Flexible RF microcoil for Neurosciences
A. Rubin1-2-3, J-C. Ginefri4, M. Tatoulian3, C. Sébrié5, B. Gillet5, L. Darrasse4, E.Dufour-Gergam2
1 Neurospin (France)
2 Paris-Sud University (France)
3 Paris VI University (France)
5 ICSN-CNRS (France)

A21 (ID 138)
A preliminary study on bio-nano-electrodes: electrochemistry and surface observation
Livia Della Seta1, Walter Vastarella1, Maria Rita Montereali1, Mihaela Ilie2-3,Vittorio Foglietti2, Roberto Pilloton1
1 ENEA(Italy)
2 CNR (Italy)
3 Politehnica Bucuresti University (Romania)

A22 (ID 141)
Microscopy and spectroscopy of SRO films with silicon nanoparticles
J. A. Luna-López1, M. Aceves-Mijares2, J. Carrillo-Lopez1, A. Morales-Sánchez2, C.Domínguez3, F. Flores-Gracia1
1 College San Manuel (Mexico)
2 INAOE (Mexico)
3 Instituto de Microelectrónica de Barcelona (Spain)

A23 (ID 153)
High-resolution miniaturized stereoscopic image sensor in CMOS technology
J. P. Carmo, R. P. Rocha, L. M. Goncalves, J. H. Correia
University of Minho (Portugal)

A24 (ID 155)
Thermoelectric batteries fabricated by a MEMS-compatible process
Jia-qi Hong, Chia-feng Chou, and Jui-che Tsa
National Taiwan University (Taiwan)

A25 (ID 173)
A novel ultra-planar, long-stroke, and low voltage piezoelectric micromirror
Thor Bakke, Ib-Rune Johansen, Andreas Vogl, Frode Tyholdt, and Dag Wang
SINTEF (Norway)

11h15 – 11h45 : Coffee break

11h45 – 13h00 : Poster session A

13h00 – 14h15 : Lunch (Palladia Hotel)

MICROSCOPY, SPECTROSCOPY AND PHOTOLUMINESCENCE OF OXIDE FILMS WITH SILICON NANOPARTICLES

J. A. Luna-López[1], M. Aceves-Mijares[2], J. Carrillo-Lopez[1], A. Morales-Sánchez[2], C. Domínguez[3], F. Flores-Gracia[1]

[1]CIDS-IC, BUAP. Ed. 103 D or C, C. U. Col. San Manuel. Puebla, Pue. México 72570.
[2]INAOE, Luis Enrique Erro No.1, Apdo. 51, Tonantzintla, Puebla, México 72000.
[3]Instituto de Microelectrónica de Barcelona, IMB-CNM (CSIC). Barcelona, Spain

Abstract
Silicon rich oxide (SRO) is a dielectric material that contains silicon nanoparticles (Si-nps). The composition, structure, and emission of the SRO films deposited by low pressure chemical vapor deposition (LPCVD) were studied; Different microscopic and spectroscopic techniques, such as Atomic Force Microscopy (AFM), High Resolution Transmission Electronic Microscopy and Energy Filtered-TEM (HRTEM and EFTEM), Rutherford Backscattering Spectroscopy (RBS), X-Ray Photoelectrons Spectroscopy (XPS) and Photoluminescence (PL) were used to characterize the SRO films. Results show that SRO films are formed by SiO_2, Si-nps, and compounds. The composition, structure (morphology and Si-nps) and luminescence of the SRO films varied with the silicon excess.

Keywords: Silicon Rich Oxide, silicon nanoparticles, Microscopy, Spectroscopy.

I- Introduction

Recently, materials that contain Si-nps have been intensively studied because of their technological importance and its excellent optoelectronic properties. One of these materials is the silicon rich oxide (SRO), where the silicon excess agglomerate creating Si-nps embedded in an oxide matrix after annealing at high temperature. The structural, electrical and optical properties of SRO films vary with the silicon excess [1, 2]. These properties have motivated the application of SRO in optoelectronics devices, such as waveguide, memories, and photodetectors [3-6]. Moreover, SRO is completely compatible with the CMOS technology. SRO films can be deposited by low pressure chemical vapor deposition (LPCVD) and many other different techniques [1-10]. LPCVD-SRO can be considered as a multi-phase material due to its is composed by a mixture of stoichiometric silicon oxide (SiO_2), not stoichiometric silicon oxide (SiO_x, $x < 2$) and elemental silicon (as Si-nps). Depending on the flow ratio (Ro) between reactant gasses and annealing time, it is possible to obtain Silicon nanocrystals (Si-ncs) < 10 nm and nanocluster ≤ 1 nm in size. Annealing is generally used to enhance the luminescent properties of the SRO films. In the present work, SRO films with different silicon excess were fabricated by LPCVD. Experimental results on the characterization of surface, volume and interface structure and PL of SRO films are presented.

II- Experiment

SRO films were deposited on N type Silicon (100) substrates with resistivity of 2-5 Ω-cm. SRO layers were obtained in a horizontal LPCVD hot wall reactor using SiH_4 (Silane) and N_2O (nitrous oxide) as reactive gases at 700 ºC. The gas flow ratio, $Ro = [N_2O]/[SiH_4] = 10$, 20 and 30, was used to control the silicon excess. After deposition the samples were densified by a thermal annealing at 1000 °C in N_2 for 30 minutes. Some of the densified samples were also thermally annealed at 1100 ºC in N_2 for 180 minutes. The surface morphology of SRO samples was studied using an easyScan Dynamic Force Microscope (DFM) Nanosurf system version 2.3, operating in a static mode. The topography for each sample was measured at a scan size of 4×4 μm^2. Five different scans were done for each sample. The average roughness and grain diameter were calculated from AFM images. The sizes of the Si-ncs and Si-nps was obtained using a Tencai F30 high resolution transmission electron microscope (HRTEM) operated with acceleration voltage of 300 kV and JEOL JEM 2010F EFTEM, respectively. The oxygen and silicon content of the as deposited SRO films was obtained

by RBS of 3.2 MeV α-particles beam of 1 mm diameter, the α-particles were obtained using the 3MV 9SDH-2 Pelletron accelerator and projectiles scattered at 168° were detected with an OXFORD 50-11 surface barrier detector.XPS data were obtained using a PHI ESCA-5500 X-ray photoelectron spectrometer with an Al radiation, E = 1486 eV. The AFM images were statistically analyzed with the software Scanning Probe Image Processor (SPIP) [11]. PL at room-temperature was measured using a Perkin-Elmer spectrometer LS-50B model with a xenon source and a monochromator. The samples were excited using 250 nm radiation, and the emission signal was collected from 400 to 900 nm with a resolution of 2.5 nm. A cutoff filter above 430 nm was used to block the light scattered from the source.

III- Results

RBS spectra of the as deposited SRO films with Ro = 20 and 30 ($SRO_{20\ and\ 30}$) are shown in Figure 1. Simulations were done with the software SIMRA version 5.02 [6] in order to analyze the RBS spectra and find the oxygen and silicon content in the films, as shown in figure 1. In both films, a small layer of SiO_2 was found at the surface of SRO films. In the SRO bulk, the silicon and oxygen ratio was determinate as 0.61/0.39 (x = 1.564) and 0.62/0.38 (x = 1.631) for $SRO_{20\ and\ 30}$, respectively. The layer thickness was finding out by RBS to be ≈ 490 nm and the superficial layer of SiO_2 is ≈ 10 nm for both samples. The simulation was done supposing differents SiO_2, SiO_x, SiO layers, until the better aproximation is obtained. Figure 2 shows the composition profile of the annealed $SRO_{20\ and\ 30}$ films obtained by XPS. A uniform Si and O content is observed inside of both SRO films. The compositions of the SRO films as measured by XPS are reported in table 1.

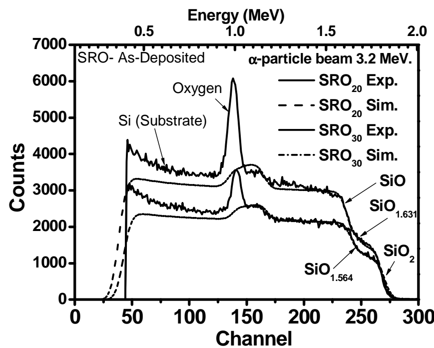

Figure 1: Experimental and simulated RBS Spectra of the $SRO_{20\ and\ 30}$ films.

Figure 3 shows the XPS Si *2p* peaks of the SRO_{10} film corresponding to the surface, volume and SRO/Si interface. A broad peak with a maximum at 104 eV is observed at the surface indicating the surface of SRO is oxidized. Besides to the 104eV peak, other peak at about 100.7 eV appears at the middle of the SRO film and it becomes more intense close to the SRO/Si interface. These broad peaks indicate the presence of different components corresponding to the different oxidation states according with the Random Bonding Model (RBM) [7-10] Moreover, both peaks at about 100.7 and 103.6 eV can be attributed to elemental Si and SiO_2, respectively, and any variation intermediate peaks are attributed to sub oxidized silicon [7-10].

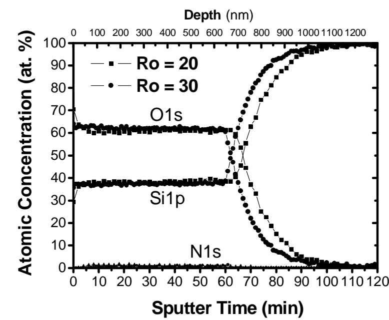

Figure 2: XPS composition profile of annealed $SRO_{20\ and\ 30}$ films.

Table 1: Composition of the SRO films, as obtained by XPS.

Ro	Thicknes s (nm)	Concentration			Si Excess %	x = O/Si
		O %	Si %	N %		
10	100	53.50	45.50	1	12.20	1.176
20	655.10	60.81	38.46	0.73	5.16	1.580
30	696.60	62.01	37.35	0.64	4.03	1.660

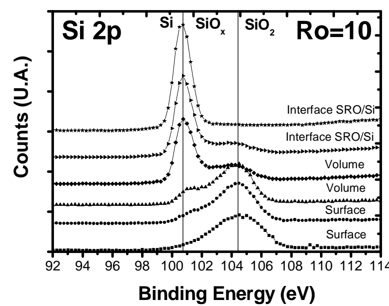

Figure 3: Si 2p XPS spectra at different position inside the SRO layer: at the surface, volume and interface of the film SRO_{10}.

The AFM images of as deposited and thermally annealed SRO films are shown in Figure 4(a) and 4(b), respectively. It can be see that the surface exhibits different characteristics depending on the Ro, which influences the size and form of the grains (roughness). The average roughness <Sa> for as-deposited SRO films with Ro = 10, 20 and 30 is 17, 10 and 8 nm, respectively. While the average roughness in annealed SRO films with Ro = 10, 20 and 30 is 24, 6 and 5 nm, respectively. The highest roughness is observed for high silicon excess (Ro = 10), which could be due to the formation of the Si-ncs or Si-nps [8].

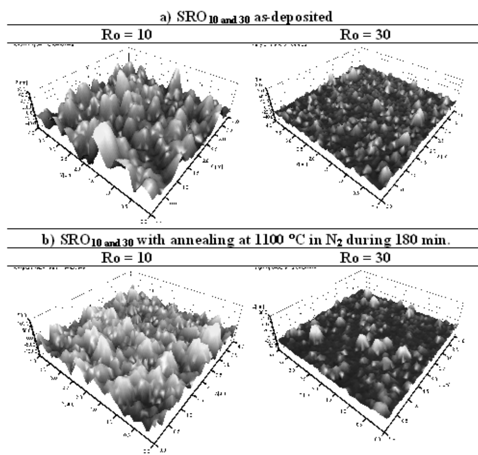

Figure 4: AFM images in 3-D of $SRO_{10\ and\ 30}$ films without and with thermal annealing.

Figure 5 shows the HRTEM and EFTEM images for the SRO films with annealing at 1100 ºC. For Ro = 10 (12.2 at. % of silicon excess), HRTEM clearly shows Si-ncs with a mean size of 5.7 nm, as shown in Figure 5(a). Si-ncs were not observed for Ro = 20 and 30. However, bright zones associated with amorphous silicon clusters were observed by EFTEM on SRO films with Ro = 20, as shown in Figure 5(b). Si-clusters with a mean size of ~2.7 nm were observed for Ro = 20, whereas for Ro = 30, because of low contrast and sharpness, the shape was not very clear, but Si-clusters with size ≤ 1 nm could be identified (not shown). Figures 6(a), 6(b), and 6(c) show the PL spectra of the as-deposited, densified, and annealed SRO films, respectively. Two PL bands can be observed: B band (400–600 nm) and A band (600–850 nm). For as-deposited SRO films, the intensity of B band increases with Ro, as shown in Figure 6(a). After densification, B band disappears and the A band becomes visible (see Figure 6(b)), prolonged annealing at higher temperature (1100° C for 180 min) enhanced its intensity, as shown in Figure 6(c). SRO films with large Ro (low Si excess) always show higher PL intensity. On the other hand, the PL peak position did not show significant shift with Ro.

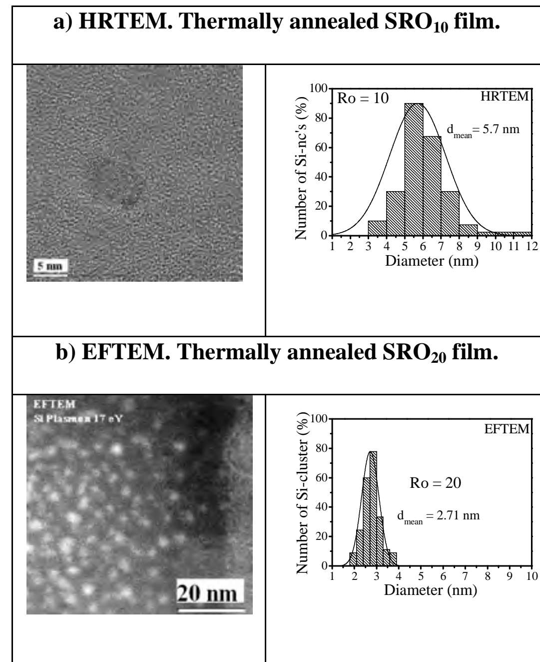

Figure 5: Silicon nanocrystal in a) SRO_{10} and silicon clusters in b) SRO_{20} films observed by HRTEM and EFTEM, respectively, after annealing at 1100 ºC.

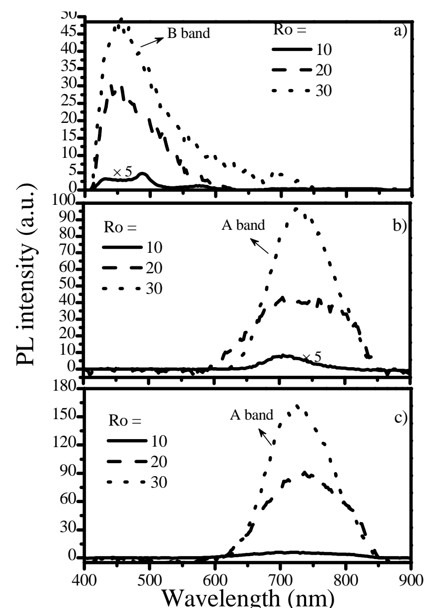

Figure 6: PL spectra measured on a) as-deposited b) densified and c) thermally annealed at 1100º C SRO films with different Ro value.

IV- Analysis and Discussion

The Si concentration of the SiO_x ($x \leq 2$) films has been obtained from RBS and XPS techniques. From XPS measurements different states of oxidation in the SRO films were observed, when the main films were deconvoluted. Table 2 show the oxidation states observed for each Ro. From here, silicon oxide (Si^{4+}) is observed in all the samples independently of the Ro. The Si^{2+} and Si^{3+} are also observed in all samples but at different depth for the different films. In the volume, the Si^{2+} is common in all samples. However, Si^{2+} and Si^{3+} are observed in the whole SRO_{30} film.
An example, for Ro = 10 is showed in Figure 3, in the surface, a broad peak corresponding to SiO_2 is observed, and in the volume, the two peaks corresponding to elemental Si and SiO_2 are a indicative of phase separation.
In HRTEM nc-Si were observed for SRO films with Ro = 10, and with lower density in Ro=20. For SRO_{30} nc-Si was not observed, but silicon agglomerates were distinguished when EFTEM was used. XPS and TEM confirm the presence of Si in the SRO for all Ro, however depending of the Ro it can be mainly crystalline or in other forms (nanoclusters), depending of the silicon excess.
In references [12-13] the authors demonstrate that in porous silicon and SiO_x the Si Plasmon energy varies. The fact that in XPS oxidation silicon states were observed, and that Si Plasmon shifts were not taken into account in our EFTEM measurements, opens the possibility that the observed silicon could be linked to oxygen forming defects, especially in the low silicon excess films.
SRO surface morphology was also studied with AFM as function of the Ro and annealing. For as deposited films the surface roughness decrease notably when the silicon excess reduces. Average roughness measured was 17, 9 and 5 nm for Ro = 10, 20 and 30, respectively. For densified and annealed samples, the roughness increases clearly in SRO_{10} from 22 to 24 nm, due to the agglomeration of Si-ncs. However, for SRO_{20}, and especially for SRO_{30} the surface from the AFM pictures looks smoother after annealing. So for low silicon excess, the elemental silicon do not exist or its density is small, with annealing the silicon agglomerate forming amorphous silicon composites rather than Si-ncs as observed from XPS and EFTEM. That is why roughness increases for Ro = 10, and reduces for higher Ro´s.

Tabla 2. *Oxidation states of the SRO films obtained by the deconvolution of the XPS curves.*

Ro	Ubication in the films	Oxidation States				
		Peak Position (eV)				
		Si^0	Si^{1+}	Si^{2+}	Si^{3+}	Si^{4+}
10	Surface				103.6	104.7
	Volume	100.7	101.7	102.9		104.1
	Interface SRO/Si	100				
20	Surface			102.5	103.4	105.5
	Volume			102.1	103.9	106
	Interface SRO/Si	100.7		102	103.8	
30	Surface		101.5		103.8	105
	Volume			102.5		104.4
	Interface SRO/Si			102.3		104.1

On the other hand, the photoluminescence also depend on Ro and thermal annealing conditions, as shown in figure 6. In our samples, intense PL (A band) in SRO_{30} was observed after annealing; however SRO_{30} has amorphous silicon composites rather than Si-ncs. On the other hand, SRO_{10} practically do not show emission, in spite that silicon nanocrystals were clearly observed before and after the annealing. Therefore, the A band cannot be associated to quantum confinement effects; instead, it should be associated to Si related defects. Also band B can be associated to defects. As reported previously [14-17], B band is also associated to F and E (different types of oxygen's vacancies) defects.

V- Conclusion

In conclusion, RBS, XPS, HRTEM and AFM were all able to measure compositional and structural differences between SRO films with different silicon excess which varied with the gas flow ratio Ro and thermal treatments. RBS and XPS allow seeing the differences on the SRO surface, in the bulk and in the SRO/Si interface as oxidation states and concentration of silicon excess. HRTEM and XPS confirmed the existence of the Si-ncs in SRO_{10}. The films consisted of three phases: Si-Si, SiO_x and SiO_2, depending on the Ro. AFM was able to analyze the surface morphology of SRO films, where the height, roughness and mean diameter of the grain and pores have a significant change with respect to the flow ratio and different annealing time. The PL also depends of the flow ratio and thermal annealing conditions.

Acknowledgment

J. Alberto Luna L. acknowledges the support received from CONACYT to through the postdoctoral scholarship. This work has been partially supported by the project 091054 from CONACYT. The authors thank Pablo Alarcón, Mauro Landa, Carlos Zúñiga,

Ignacio Juárez and Netzhualcoyotl Carlos for helping in the preparation of the samples.

References

[1] L. Pavesi, L. Dal Negro, L. Mazzoleni, G. Franzo, and F. Priolo, Nature, vol.408, pp440, 2000.
[2] O. Hanaizumi, K. Ono, and Y. Ogawa, Appl. Phys. Lett, vol.82, pp.538-540, 2003.
[3] Y. C. Fang, W. Q. Li, L. J. Qi, L. Y. Li, Y. Y. Zhao, Z. J. Zhang, and M. Lu, Nanotechnology, vol.15, pp.495-500, 2004.
[4] D. Dong et al, J.Electrochem. Soc., vol.125, pp.819-823,1978.
[5] P. G. Pai, S. S. Chao, and Y. Takagi, J. Vac. Sci. Technol., vol.A4, p.689, 1986.
[6] Mayer Matej, Software SIMNRA versión 5.02, Max Plank-Institute für Plasmaphysik, D-85748 Garching, Germany, 1997-2004.
[7] Fabio Iacona, Glorgia Franzo, and Corrado Spinella, J. Appl. Phys., vol.87, p.1295, 2000.
[8] Fabio Iacona, Corrado Borgiono, and Corrado Spinella, J. Appl. Phys., Vol. 95, No. 7, p. 3723-3732, 2004.
[9] Shinji Hayashi, Shinichi Tanimoto and Keiichi Yamamoto, J. Appl. Phys.,Vol. 68, No. 10, p. 5300-5308, 1990.
[10] L.B. Mag, A.L. Ji, C. Liu, Y. Q. Wang and Z.X. Cao, J. Vac. Sci. Technol. B, Vol. 22, No. 6, p. 2654-2657, 2004.
[11] The Scanning Probe Image Processor (SPIP), image metrology www.imagemet.com., 2005.
[12] N. Mannella, G. Gabetta, F. Parmigiani, Appl. Phys. Lett., Vol. 79, No. 26, pp. 4432–4434, 2001.
[13] Yang Lin, Liu Yu-Liang, Wang Qi-Ming, Li Guang-Hai Zhang Li-De, Chin. Phys. Lett., Vol. 19, No. 6, 867, (2002).
[14] K. H. Lee and J. H. Crawford, Jr., Luminescence of the F center in sapphire, Physical Review B, 19 (6), 3217 (1979).
[15] K. Sato and K. Hirakuri, J. Appl. Phys. 100, 114303-1 (2006).
[16] Gong-Ru Lin, Chun-Jung Lin, and Chi-Kuan Lin, J. Appl. Phys. 97, 094306-1 (2005).
[17] Chung-Jung Lin and Gong-Ru Lin, IEEE J. Quant. Elect., 41 (3), 441 (2005).
[17] D. J. DiMaria, J. R. Kirtley, E. J. Pakulis, D. W. Dong, T. S. Kuan, F. L. Pesavento, T. N. Theis, J. A. Cutro, and S. D. Brorson, *J. Appl. Phys.* **56** (2), 401 (1984).
[18] T. V. Torchynska, *J. Appl. Phys.* **92,** 4019 (2002).